7238 *Macromolecules* **2010**, *43*, 7238–7243
DOI: 10.1021/ma902471g

Macromolecules
ARTICLE

Toughening of Epoxies with Block Copolymer Micelles of Wormlike Morphology

Jia (Daniel) Liu,[†,⊥] Zachary J. Thompson,[‡] Hung-Jue Sue,*[,†] Frank S. Bates,[‡] Marc A. Hillmyer,[§] Marv Dettloff,[∥] George Jacob,[∥] Nikhil Verghese,[∥] and Ha Pham[∥]

[†]*Polymer Technology Center, Department of Mechanical Engineering, Texas A&M University, College Station, Texas 77843,* [‡]*Department of Chemical Engineering and Materials Science, and* [§]*Department of Chemistry, University of Minnesota, Minneapolis, Minnesota 55455, and* [∥]*The Dow Chemical Company, Epoxy R&D, Freeport, Texas 77541.* [⊥]*Current affiliation: Exponent, Inc. Tel: (301) 291-2504. E-mail: djliu@exponent.com.*

Received November 8, 2009; Revised Manuscript Received June 23, 2010

ABSTRACT: An amphiphilic poly(ethylene-*alt*-propylene)-*b*-poly(ethylene oxide) (PEP-PEO) block copolymer (BCP) was blended with a bisphenol A-based epoxy resin formulation and self-assembled into a wormlike micelle structure. With an incorporation of 5 wt % of the BCP material, the fracture toughness was improved by >100% over the neat epoxy. The morphology and mechanical properties of this BCP-modified epoxy were investigated using transmission electron microscopy, dynamic mechanical analysis, tensile tests, and fracture toughness measurements. Toughening mechanisms from the wormlike micelle-modified material were investigated using the double-notch four-point-bending technique, and the results are compared with data obtained from the same epoxy thermoset formulation containing a BCP that self-assembled into spherical micelles. Elongated cylindrical micelles produce improved toughness, which is interpreted on the basis of a combination of mechanisms including crack tip blunting, cavitation, particle debonding, limited shear yielding, and crack bridging. The implications of the present study for polymer toughening in general are also discussed.

1. Introduction

Block copolymers (BCPs) have been shown to be highly effective at improving epoxy mechanical properties.[1−17] At low concentrations in epoxy resins, a BCP may self-assemble into well-defined micro/nanostructures in the form of three distinct morphologies: spherical micelles, wormlike micelles, and vesicles. The type of structure formed depends on the molecular weight, block length, composition, and block−block and block−matrix interaction parameters.[11] These morphologies mimic those of the BCP when dispersed in selective solvents[18−24] or homopolymers.[25−29] When the solvent or the homopolymer is highly selective for one block, symmetric BCPs form spherical micelles in the dilute limit, whereas asymmetric BCPs form either wormlike micelles or vesicles. In thermosetting systems, the phase behavior is primarily guided by the same fundamental physics operative in solvents and in homopolymer blends, which involves selective solvation of the miscible block.[1−4,6,24]

Although BCPs previously have been studied as toughening agents with epoxy resins,[1−11] most of the BCP studied are in the form of spherical micelles. Only a limited number of investigations have addressed other self-assembled morphologies, especially the wormlike micelles, attributable to a narrow BCP composition window needed to control and stabilize the wormlike micelle structure. In addition, there have been inconsistent results in the toughening effects from BCP structures with different morphologies.[7] For both fundamental research and commercial applications, it is necessary to explore fully the ability of BCP to produce morphologies other than spherical micelles and to investigate their influences on the mechanical properties of cured epoxy matrices.

In our previous publications,[14−17] we have discussed in detail the mechanical properties and toughening mechanisms of a model DGEBA epoxy resin thermoset modified with poly(ethylene-*alt*-propylene)-*b*-poly(ethylene oxide) (PEP-PEO) amphiphilic BCP that forms 15 nm diameter spherical micelles. The addition of this BCP toughening agent can improve the epoxy fracture toughness by as much as 180%. The major operative toughening mechanism in the modified epoxies has been found to be BCP micelle particle cavitation-induced matrix shear banding. In the current work, focus is placed on the mechanical properties and fracture behavior of an epoxy resin thermoset composition modified with 5 wt % of a PEP-PEO BCP that yields wormlike micelles. We achieved this morphology by tuning the molecular weight and poly(ethylene oxide) (PEO) fraction of the PEP-PEO copolymer and the cross-link density of the epoxy matrix. Fracture toughness (K_{IC}, critical stress intensity factor) measurements, tensile tests, and dynamic mechanical analysis (DMA) results are presented and compared with the same epoxy resin that contains spherical micelles. The implications of the present study for polymer toughening in general are also discussed.

2. Experimental Section

2.1. Materials. Diglycidyl ether of bisphenol A (DGEBA) epoxy resin (D.E.R. 332, Dow Chemical), 1,1,1-tris(4-hydroxyphenyl)ethane (THPE, Aldrich), and bisphenol A (BPA, PARABIS, Dow Chemical) were used as the matrix, cross-linker, and difunctional chain extender, respectively. Ethyltriphenylphosphonium acetate (70% in methanol, Alfa Aesar) was added as a catalyst to reduce the cure time.

*To whom correspondence should be addressed. Tel: (979) 845-5024. E-mail: hjsue@tamu.edu.

 Published on Web 08/06/2010

The PEP-PEO diblock copolymer was synthesized using a multistep polymerization approach.[30] The weight fraction of EO, w_{EO}, in the BCP was tuned to 0.32. The number-average molecular weight, M_n, and the polydispersity index, PDI, of the BCP were 7300 g/mol and 1.06, respectively. For comparison purposes, the BCP that gave spherical micelles had a w_{EO} of 0.40 and an M_n of 9100 g/mol. In epoxy thermosets, PEO is the miscible block and PEP is the immiscible block.

2.2. Preparation of BCP Wormlike Micelle-Modified Epoxy. Samples were prepared by solvent casting. A detailed sample preparation procedure is described elsewhere.[17] The BCP was first completely dissolved in acetone and mixed with the epoxy monomer, the cross-linker, and the chain extender. The solvent was then removed under dynamic vacuum, first at room temperature and then gradually heating to 130 °C. Catalyst was then added, and the mixture was cured in an oven at 200 °C for 2 h.

Various molecular weights between cross-links (M_c) of the epoxy thermoset compositions were prepared and evaluated, but the long wormlike morphology was only obtained in the system with a theoretical M_c of 600 g/mol. The total concentration of BCP in the material was 5 wt %. All specimens were completely dried in a vacuum oven at 80 °C for over 24 h before morphological and mechanical characterizations.

For comparison purpose, a BCP spherical micelle-modified epoxy was also prepared with the same M_c (600 g/mol). The neat epoxy, BCP wormlike micelle-modified epoxy, and BCP spherical micelle-modified epoxy are designated as CET600, CET600/worm, and CET/sphere, respectively.

2.3. Transmission Electron Microscopy (TEM). The morphological characterization of CET600/worm was performed using TEM. Cured epoxy plaques were first microtomed at room temperature using a Reichert Ultracut E Ultramicrotome and a Micro Star diamond knife, and ultrathin sections (ca. 70 nm in thickness) were collected on a copper grid. These thin sections were vapor-stained with a fresh 0.5 wt % RuO_4 aqueous solution for 8−10 min at room temperature and subsequently examined using a JEOL 1210 EX electron microscope operated at an accelerating voltage of 120 kV.

2.4. Dynamic Mechanical Analysis. DMA was performed using an ARES-G2 instrument (TA Instruments) with a torsional fixture using specimen dimensions of $40 \times 12.7 \times 3.5\ mm^3$. Tests were run from −120 to 200 °C with temperature increases of 5 °C per step and a fixed frequency of 1 Hz. A sinusoidal strain amplitude of 0.05% was chosen for the analysis. The dynamic storage modulus (G') and tan δ curves were plotted as a function of temperature. We interpret the peak in tan δ ($= G''/G'$) as the glass-transition temperature (T_g).

2.5. Tensile Tests. Room-temperature tensile tests were conducted in accordance with ASTM D638-98, using an MTS servo-hydraulic test machine at a crosshead speed of 5.08 mm/min. Strain was measured using a calibrated MTS extensometer (Model 632.11B-20). Young's modulus, tensile strength, and elongation at break were obtained on the basis of at least five specimens per sample. Average values and standard deviations were reported.

2.6. Fracture Toughness Measurements. Fracture toughness measurements were performed following the linear elastic fracture mechanics (LEFM) approach. A single-edge-notch three-point-bending (SEN-3PB) test was used to obtain the K_{IC} in accordance with ASTM standard D5045. The dimensions of specimens are $75 \times 12.7 \times 3.5\ mm^3$. The tests were performed on an MTS Insight machine at a test speed of 0.508 mm/min. Care was taken to ensure that the initial crack, generated by tapping with a fresh razor blade chilled with liquid N_2, exhibited a thumbnail shape crack front prior to testing. Five specimens were used to determine the K_{IC} of the samples.

2.7. Double-Notch Four-Point-Bending (DN-4PB) Test. To gain a fundamental understanding of the toughening mechanisms, the DN-4PB test[31] was employed to probe the detailed micromechanical deformation of BCP-toughened epoxy upon fracture.

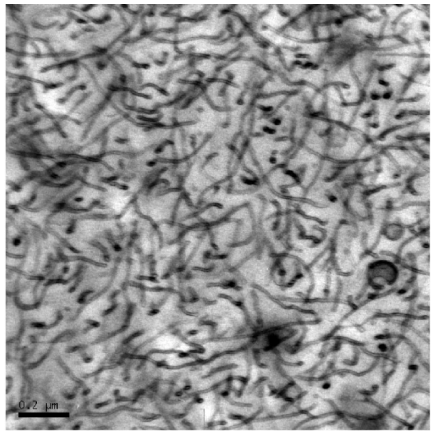

(a)

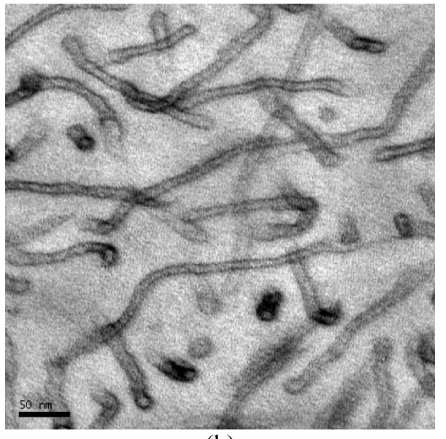

(b)

Figure 1. TEM micrographs of BCP wormlike micelle-modified epoxy at (a) low magnification and (b) high magnification.

Complete descriptions and schematics of the DN-4PB technique can be found elsewhere.[14]

DN-4PB tests were conducted at room temperature on an MTS Insight machine. A specimen was loaded in a four-point bending geometry with the cracks positioned on the tensile side. The test rate was chosen to be 0.508 mm/min. The arrested subcritical crack tip damage zone from the core region of the specimen was diced off and prepared accordingly for optical microscopy (OM) and TEM observations.

For OM investigations, thin sections of the midsection of the DN-4PB crack tip damage zone were obtained by cutting and polishing to a thickness of ca. 40 μm. These thin sections were then examined using an Olympus BX60 optical microscope under both bright and cross-polarized light fields.

For TEM imaging, a block with the crack tip damage zone was isolated from the specimen and embedded in Epo-Fix embedding resin for ultramicrotoming use (Electron Microscopy Sciences). After curing overnight at room temperature, the block was trimmed into a trapezoid shape at the tip with a cross section area of around $0.3 \times 0.3\ mm^2$. Then, the trimmed block was faced off by a Micro Star diamond knife, followed by microtoming and staining as aforementioned. The TEM imaging was carried out using a JEOL 1200 EX electron microscope operated at an accelerating voltage of 100 kV. TEM beam damage was minimized during these experiments.

3. Results and Discussion

3.1. Morphology of BCP Wormlike Micelle-Modified Epoxy. The transparency of the epoxy containing wormlike micelles is similar to the one with spherical micelles. TEM micrographs of the RuO_4-stained sample, shown in Figure 1,

reveal well-defined PEP-PEO-based wormlike micelles that are homogeneously dispersed in epoxy. Here epoxy-philic PEO block forms a corona structure surrounding the epoxy-phobic PEP core. The PEO-rich region looks slightly darker than the PEP cores in the TEM micrographs, and they appear to form a tubular structure with a diameter of ca. 10−15 nm. No macroscopic phase separation or agglomerates were observed.

3.2. Dynamic Mechanical Analysis. DMA data obtained from CET600, CET600/sphere, and CET600/worm, are presented in Figure 2, and the storage modulus and T_g values are summarized in Table 1. CET600/sphere and CET600/worm samples exhibit very similar dynamic mechanical behavior, and they both have almost no reduction in T_g and storage modulus compared with CET600 at temperatures below 25 °C. In fact, the CET600/worm specimen has a slightly higher storage modulus than the neat resin counterpart at temperatures below −100 °C. However, both CET600/sphere and CET600/worm have a progressive reduction in storage modulus at temperatures above 25 °C. Most noticeably, both CET600/sphere and CET600/worm samples exhibit higher tan δ values than those of CET600 between the α and β transition peaks. This suggests that both the spherical and wormlike BCP micelles have either participated in the epoxy network formation or influenced network molecular mobility, causing increased damping characteristics of the BCP-modified epoxies. This finding indicates that the addition of the BCP phase enhances the energy dissipation capacity of the epoxy matrix, rendering the matrix more viscoelastic at temperatures above 25 °C.

3.3. Tensile Behavior. Representative engineering stress−true strain curves, associated with data taken from CET600, CET600/sphere, and CET600/worm, are plotted in Figure 3. Average values of the Young's modulus, tensile strength and elongation at break are summarized in Table 2. The addition of BCP to the epoxy causes only a slight reduction in the Young's modulus at room temperature. However, the presence of wormlike micelles results in a pronounced increase in the tensile strength and elongation at break. These improvements are not observed to the same extent with the spherical micelle-modified epoxy. Upon comparison with CET600 and CET600/sphere, it is obvious that the CET600/wWorm material exhibits a dramatically improved ductility and toughness, along with a slight increase in strength. This tensile property improvement is likely caused by the presence of the wormlike micelles and the surrounding epoxy network that might be modified by the corona PEO blocks. At this moment, we are uncertain how the BCP micelles affect the surrounding epoxy network formation and its corresponding deformation mechanisms. How the spherical micelles and wormlike micelles differ in influencing the interfacial characteristics and the surrounding epoxy network formation remains an open question. Nevertheless, the modification of epoxy with BCP wormlike micelles appears to be a promising approach for obtaining high-performance engineering polymers with attractive mechanical characteristics.

3.4. Fracture Toughness Measurements. The K_{IC} values of CET600, CET600/sphere, and CET600/worm are summarized in Table 3. An improvement in K_{IC} by 106% over the neat epoxy is observed for the CET600/worm sample. This improvement is remarkable considering the fact that the total loading of BCP is only 5 wt % and the CET600 has a relatively high cross-link density. In contrast, the spherical micelles are relatively less effective in toughening epoxy networks. To investigate why the wormlike micelles are more effective for epoxy toughening, the fracture mechanisms of CET600/worm were probed. It is also noted that the fracture toughness value of CET/worm has a noticeably higher standard deviation than the two control samples. This is probably due to the fact that the natural crack tip radius of epoxy is of the same order as the length of the wormlike structure (~0.5 μm). Depending on exactly where the crack tip is located with respect to the wormlike structure, the resistance against crack propagation would vary. In contrast, for epoxies without BCP or the mixtures containing the 15 nm spherical micelles, the location of the crack tip with

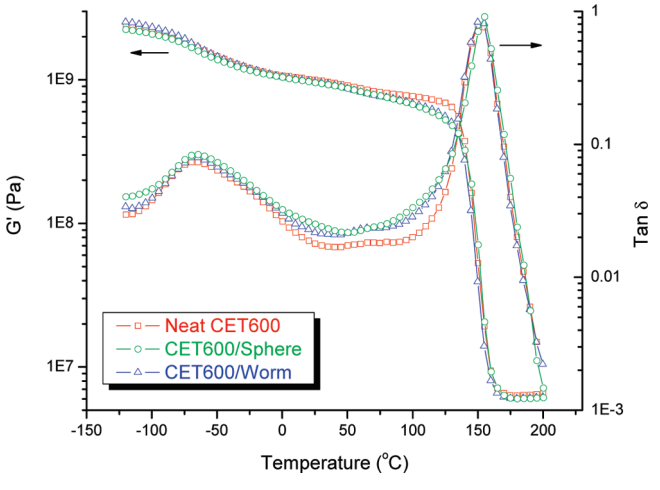

Figure 2. DMA plots of CET600, CET600/sphere, and CET600/worm. Storage modulus (G') and tan δ curves as a function of temperature are presented.

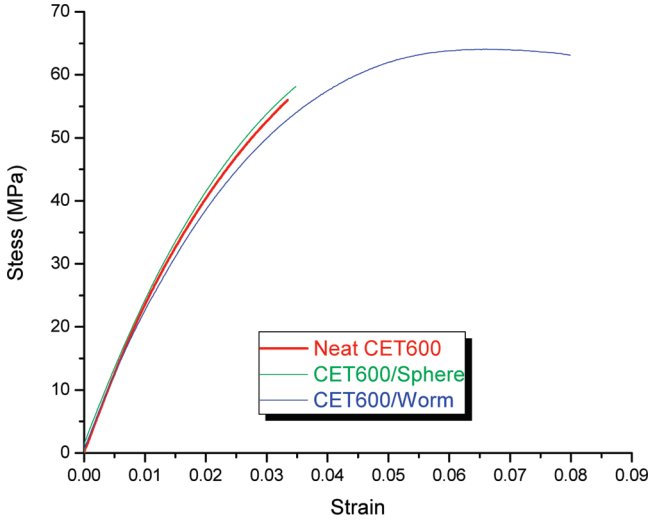

Figure 3. Representative engineering stress−true strain curves of CET600, CET600/sphere, and CET600/worm.

Table 1. Storage Modulus and T_g Values of CET600, CET/sphere, and CET/worm

		CET600	CET600/sphere	CET600/worm
T_g (°C)		152	155	152
storage modulus (Pa)	at −100 °C	2.23×10^9	2.08×10^9	2.33×10^9
	at 25 °C	1.00×10^9	9.56×10^8	9.70×10^8
	at rubbery plateau (T_g + 50 °C)	6.54×10^6	6.12×10^6	6.20×10^6

Table 2. Average Values of Young's Modulus, Tensile Strength and Elongation at Break of CET600, CET600/Sphere, and CET600/Worm

	CET600	CET600/sphere	CET600/worm
Young's modulus (GPa)	2.56 ± 0.02	2.42 ± 0.05	2.44 ± 0.03
tensile strength (MPa)	58.7 ± 3.7	58.1 ± 1.2	63.7 ± 0.6
elongation at break (%)	3.6 ± 0.4	3.5 ± 0.3	8.0 ± 0.9

Table 3. Fracture Toughness K_{IC} (MPa·m$^{1/2}$) of CET600, CET600/Sphere, and CET600/Worm

	CET600	CET600/sphere	CET600/worm
K_{IC} (MPa·m$^{1/2}$)	0.87 ± 0.04	1.60 ± 0.04	1.79 ± 0.12
relative increase		+84%	+106%

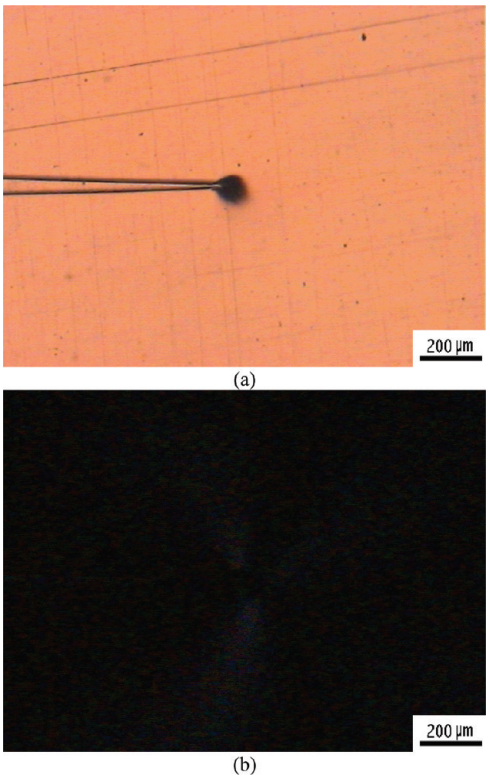

Figure 4. OM images of the DN-4PB specimen of CET600/worm with the subcritical crack tip damage zone under (a) bright field and (b) cross-polarized light field. The crack propagates from left to right.

respect to the micelle particles becomes irrelevant. This leads to more consistent fracture toughness results.

3.5. Toughening Mechanisms Investigation. We further investigated the toughening mechanisms of the BCP wormlike micelle-toughened epoxy network by examining the crack tip damage zone of the DN-4PB specimens using OM and TEM.

The OM micrographs of the damage zone under bright field and cross-polarized light field are shown in Figures 4a,b, respectively. Evidence of the cavitation process in CET600/worm is presented in Figure 4a. The size of the cavitation zone is ~60 μm in diameter. Under cross-polarized light, little or no birefringent zone was found. This indicated that either the shear banding zone size in CET600/worm is very small or the presence of the wormlike micelle prevents the formation of permanent plastic deformation of the epoxy matrix around the crack tip region. Either way, other toughening mechanisms, such as crack tip blunting and viscoelastic energy dissipation, may be at play as well.[14]

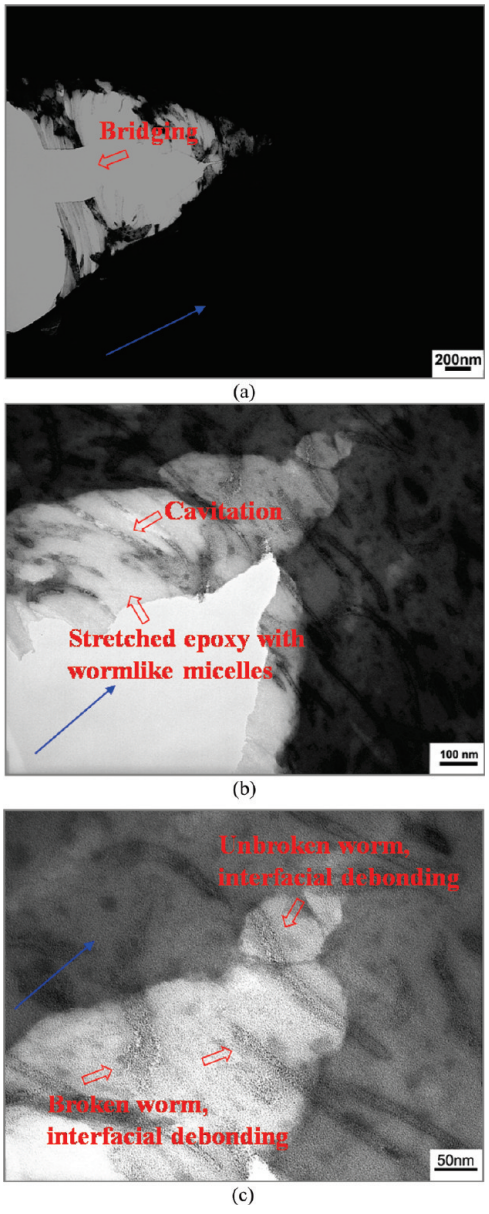

Figure 5. TEM micrographs of the crack tip DN-4PB specimen of BCP-toughened epoxy: (a) overview of the crack tip, (b) evidence of wormlike structure cavitation or fragmentation after severe stretching, and (c) evidence of interfacial debonding or voiding. The blue arrows in the micrographs indicate the direction of crack propagation.

To establish unambiguously the mechanisms responsible for the observed toughening effect, a TEM investigation was performed.

TEM micrographs were taken at the subcritical crack tip region of the DN-4PB specimens. As shown in Figure 5a, it is evident that the wormlike micelles bridge between the opening crack planes. Because the micrograph was taken based on the unloaded specimen, it is uncertain if the wormlike domains were stretched during loading. If so, it might help contribute to the observed toughening effect. A higher magnification observation at the crack tip region (Figure 5b) further reveals the morphology of the stretched, thinned epoxy matrix that contained wormlike micelles at the edge of the crack, which is indicative of the high ductility of the CET600/worm. This enhanced matrix ductility is consistent with the tensile behavior of this epoxy system. (See Figure 3 and Table 2.)

Careful investigation of the micrographs reveals cavitation of the soft rubber inside the wormlike micelles in this stretched epoxy region. Interestingly, at the very tip region of the crack where the epoxy has been thinned but not yet broken (Figure 5c), both "broken worms" and "unbroken worms" are found bridging the crack tip. The "unbroken worms" are likely to be broken if the crack further opens up. It is interesting to note that both ends of the "broken worms" appear to have been stretched when the crack develops. Meanwhile, partial interfacial debonding or voiding is observed around both "broken worms" and "unbroken worms", which is not seen in the case of spherical micelle-modified epoxies.[14−16] We speculate that such debonding or voiding occurs mainly because of the relatively short EO block length of the BCP at the interface, causing disentanglement of the BCP upon stretching. These cavitation, voiding, and debonding mechanisms in the epoxy network likely account for the observed cavitation zone in OM (Figure 4a).

It is noted that the apparent cavitation/voiding/debonding mechanisms shown by the OM are not completely observed via TEM investigation. This discrepancy could be due to stress relief upon ultrathin sectioning of the specimen, the small size of the cavitational features, or both. It should also be noted that TEM observes only a 2-D projection of 60−80 nm thick thin sections, whereas OM takes into account a 2-D projection of ∼100 μm thick sections of the sample. To establish conclusively the sequence of toughening events, a more sophisticated technique like in situ TEM is probably required.

On the basis of the evidence presented here, we believe the improvement in fracture toughness is likely to derive from a combination of several toughening mechanisms: voiding or debonding at the interface between the phases, limited matrix shear yielding, crack tip blunting, crack bridging, and viscoelastic energy dissipation. However, it is worth mentioning that none of these mechanisms alone dominates the fracture energy dissipation process in this case. As previously reported,[16] the CET900/sphere sample with a theoretical M_c of 900 g/mol exhibited very limited cavitation and matrix shear yielding at the crack tip region upon fracture. Therefore, for CET600/sphere that possesses an even higher matrix cross-link density, the effectiveness of the cavitation-induced shear yielding mechanism on toughening is expected to be minimal. Meanwhile, interfacial debonding or crack bridging is likely to be negligible because of the small size of the spherical micelle particles with respect to the crack tip radius.[34] Consequently, the CET600/sphere material exhibits a lower fracture toughness value than the CET600/worm sample.

Creating wormlike micelle structures in epoxy networks is not straightforward because the composition window for successfully controlling and stabilizing the formation of this morphology is very narrow.[17] Care must be taken in choosing an appropriate EO fraction, w_{EO}. A lack of precise control in synthesizing the BCP will result in the formation of spherical micelles or vesicles rather than the desired wormlike micelles.

The formation of wormlike micelles seems to be dependent on the nature and the cross-link density of the epoxy matrix. As previously mentioned, in this particular system, only the epoxy resin with M_c of 600 g/mol contained wormlike micelles. Spherical micelles, elongated ellipsoid micelles, disklike micelles, or larger size vesicle-like structures are usually seen in epoxies with higher M_c. Different epoxy compositions seem to influence the formation of wormlike micelles as well. Fundamental knowledge on how the formulation and the cross-link density of the epoxy resin composition affect the formation of disordered BCP morphologies is not yet fully developed and needs to be further investigated.

Finally, on the basis of this study, it appears that the wormlike BCP micelle structure is most effective for improving the ductility and toughness of highly cross-linked epoxy networks. The DMA results suggest that both the spherical micelle particles and the wormlike micelle structure have a similar effect on altering the damping behavior of the epoxy matrix. The operative toughening mechanisms discussed above also suggest that the toughening effect can be attributed to many mechanisms and factors. However, we cannot make definitive claims at this point regarding the precise contribution of each mechanism to the overall improvement in fracture toughness, mainly because shear yielding appears to be highly constrained in the epoxy matrix, and other toughening mechanisms, such as crack bridging, are not easily quantified in this system. It is still uncertain how the wormlike structure improves the mechanical properties of highly cross-linked epoxies. Another plausible explanation of the wormlike micelle structure, over that of the spherical micelle particles, is the formation of a unique epoxy network structure with certain asymmetric distribution of cross-links around the wormlike structures. This could lead to improved ductility of the epoxy matrix, as evidenced by the thinned and stretched epoxy matrix at the crack tip region (Figure 5) and the associated tensile behavior (Figure 3). This conjecture awaits further validation and will be the subject of future investigations.

4. Conclusions

A PEP-PEO (M_n = 7500 g/mol, w_{EO} = 0.32) amphiphilic BCP was used to modify a DGEBA-type of epoxy resin. The BCP molecules self-assemble into well-dispersed wormlike micelles with a diameter of 10−15 nm. The epoxy-miscible PEO block forms a corona surrounding the epoxy-immiscible PEP core. Incorporation of 5 wt % BCP wormlike micelles gives a 100% improvement in K_{IC}, which is more effective than that of the spherical micelle-modified epoxy. In comparison with the neat epoxy counterpart, wormlike micelle-modified epoxy can concurrently improve tensile properties without compromising T_g and modulus. Key operative toughening mechanisms have been identified to be crack tip blunting, cavitation, debonding (voiding), limited shear yielding, and crack bridging.

Acknowledgment. This research was funded by the Dow Chemical Company. Partial financial support from the Department of Energy through a subcontract to UT-Battelle (no. 4000041622) is also gratefully acknowledged by Z.J.T. and F.S.B.

References and Notes

(1) Hillmyer, M. A.; Lipic, P. M.; Hajduk, D.; Almdal, K.; Bates, F. S. *J. Am. Chem. Soc.* **1997**, *119*, 2749.
(2) Lipic, P. M.; Bates, F. S.; Hillmyer, M. A. *J. Am. Chem. Soc.* **1998**, *120*, 8963.
(3) Grubbs, R. B.; Broz, M. E.; Dean, J. M.; Bates, F. S. *Macromolecules* **2000**, *33*, 2308.
(4) Grubbs, R. B.; Broz, M. E.; Dean, J. M.; Bates, F. S. *Macromolecules* **2000**, *33*, 9522.
(5) Dean, J. M.; Lipic, P. M.; Grubbs, R. B.; Cook, R. F.; Bates, F. S. *J. Polym. Sci., Part B: Polym. Phys.* **2001**, *39*, 2996.
(6) Grubbs, R. B.; Dean, J. M.; Bates, F. S. *Macromolecules* **2001**, *34*, 8593.
(7) Dean, J. M.; Grubbs, R. B.; Saad, W.; Cook, R. F.; Bates, F. S. *J. Polym. Sci., Part B: Polym. Phys.* **2003**, *41*, 2444.
(8) Dean, J. M.; Verghese, N. E.; Pham, H. Q.; Bates, F. S. *Macromolecules* **2003**, *36*, 9267.

(9) Guo, Q.; Dean, J. M.; Grubbs, R. B.; Bates, F. S. *J. Polym. Sci., Part B: Polym. Phys.* **2003**, *41*, 1994.
(10) Sumeet, J.; Bates, F. S. *Science* **2003**, *300*, 460.
(11) Wu, J.; Thio, Y. S.; Bates, F. S. *J. Polym. Sci., Part B: Polym. Phys.* **2005**, *43*, 1950.
(12) Girard-Reydet, E.; Pascault, J.-P.; Bonnet, A.; Court, F.; Leibler, L. *Macromol. Symp.* **2003**, *198*, 309.
(13) Hydro, R. M.; Pearson, R. A. *J. Polym. Sci., Part B: Polym. Phys.* **2007**, *45*, 1470.
(14) Liu, J.; Sue, H.-J.; Thompson, Z. J.; Bates, F. S.; Dettloff, M.; Jacob, G.; Verghese, N.; Pham, H. *Macromolecules* **2008**, *41*, 7616.
(15) Liu, J.; Sue, H.-J.; Thompson, Z. J.; Bates, F. S.; Dettloff, M.; Jacob, G.; Verghese, N.; Pham, H. *Acta. Mater.* **2009**, *57*, 2691.
(16) Liu, J.; Sue, H.-J.; Thompson, Z. J.; Bates, F. S.; Dettloff, M.; Jacob, G.; Verghese, N.; Pham, H. *Polymer* **2009**, *50*, 4683.
(17) Thompson, Z. J.; Hillmyer, M. A.; Liu, J.; Sue, H.-J.; Dettloff, M.; Bates, F. S. *Macromolecules* **2009**, *42*, 2333.
(18) Zhang, L.; Eisenberg, A. *Science* **1995**, *268*, 1728.
(19) Hajduk, D. A.; Kossuth, M. B.; Hillmyer, M. A.; Bates, F. S. *J. Phys. Chem. B* **1998**, *102*, 4269.
(20) Alexandridis, P.; Spontak, R. J. *Curr. Opin. Colloid Interface Sci.* **1999**, *4*, 130.
(21) Discher, B. M.; Won, Y. Y.; Ege, D. S.; Lee, J. C.-M.; Bates, F. S.; Discher, D. E.; Hammer, D. A. *Science* **1999**, *284*, 1143.
(22) Discher, B. M.; Hammer, D. A.; Bates, F. S.; Discher, D. E. *Curr. Opin. Colloid Interface Sci.* **2000**, *5*, 125.
(23) Lodge, T. P.; Pudil, B.; Hanley, K. J. *Macromolecules* **2002**, *35*, 4707.
(24) Won, Y. Y.; Brannan, A.; Davis, H. T.; Bates, F. S. *J. Phys. Chem. B* **2002**, *106*, 3354.
(25) Kinning, D. J.; Winey, K. I.; Thomas, E. L. *Macromolecules* **1988**, *21*, 3502.
(26) Kinning, D. J.; Thomas, E. L.; Fetters, L. J. *Macromolecules* **1991**, *24*, 3893.
(27) Koizumi, S.; Hasegawa, H.; Hashimoto, T. *Makromol. Chem. Macromol. Symp.* **1992**, *62*, 75.
(28) Matsen, M. W. *Macromolecules* **1995**, *28*, 5765.
(29) Bates, F. S.; Maurer, W. W.; Lipic, P. M.; Hillmyer, M. A.; Almdal, K.; Mortensen, K.; Fredrickson, G. H.; Lodge, T. P. *Phys. Rev. Lett.* **1997**, *79*, 849.
(30) Hillmyer, M. A.; Bates, F. S. *Macromolecules* **1996**, *29*, 6994.
(31) Sue, H.-J.; Yee, A. F. *J. Mater. Sci.* **1993**, *28*, 2975.